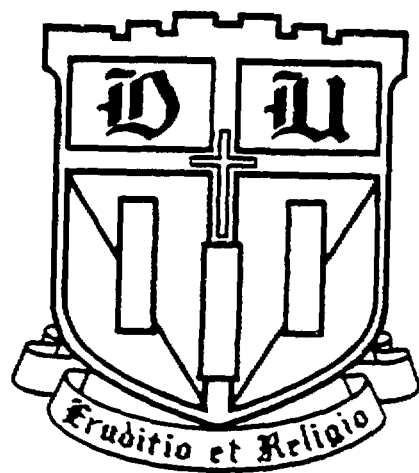


(CONF-8909447--1)

CONF-8909447--1

DE91 018389



DEPARTMENT OF PHYSICS

Duke University

Durham, North Carolina 27706

DISCLAIMER

This report was prepared as an account of work sponsored by an agency of the United States Government. Neither the United States Government nor any agency thereof, nor any of their employees, makes any warranty, express or implied, or assumes any legal liability or responsibility for the accuracy, completeness, or usefulness of any information, apparatus, product, or process disclosed, or represents that its use would not infringe privately owned rights. Reference herein to any specific commercial product, process, or service by trade name, trademark, manufacturer, or otherwise does not necessarily constitute or imply its endorsement, recommendation, or favoring by the United States Government or any agency thereof. The views and opinions of authors expressed herein do not necessarily state or reflect those of the United States Government or any agency thereof.

Relativistic Heavy Ion Physics

Berndt Müller*

Department of Physics, Duke University, Durham, NC 27706

Abstract

Central nuclear collisions at energies far above 1 GeV/nucleon may provide for conditions, where the transition from highly excited hadronic matter into quark matter or quark-gluon plasma can be probed. We review current ideas about the nature of, and signals for, this transition, and we discuss the (hadronic) string model approach to the nuclear collisions dynamics. At even higher energies in the TeV/nucleon range peripheral nuclear collisions may become a laboratory for electroweak physics at the unification scale allowing, e.g., for Higgs boson production.

*Invited lecture presented at the Third Hellenic School on Elementary Particle Physics, Corfu, Greece, 13-30 September 1989.

DISTRIBUTION OF THIS DOCUMENT IS UNLIMITED

MASTER

FG05-90ER40592

RELATIVISTIC HEAVY ION PHYSICS

Berndt Müller

Department of Physics, Duke University, Durham, NC 27706

ABSTRACT

Central nuclear collisions at energies far above 1 GeV/nucleon may provide for conditions, where the transition from highly excited hadronic matter into quark matter or quark-gluon plasma can be probed. We review current ideas about the nature of, and signals for, this transition, and we discuss the (hadronic) string model approach to the nuclear collisions dynamics. At even higher energies in the TeV/nucleon range peripheral nuclear collisions may become a laboratory for electroweak physics at the unification scale allowing, e.g., for Higgs boson production.

1. INTRODUCTION

After a collision between ^{16}O nucleus of 3200 GeV total energy and a ^{197}Au nucleus several hundred charged particles are emitted. No one in his or her right mind would care to study such events, unless there existed a compelling reason for it. The current interest in nuclear collisions at very high energies (far above 1 GeV/u in the c.m. system) is fueled by the expectation that a *quark gluon plasma* may be created temporarily in these events [1-3]. Whereas there is general consensus among theorists that QCD thermodynamic equilibrium exhibits a phase transition from the normal color-confined phase of hadronic matter with broken chiral symmetry to a deconfined, chirally symmetric phase at sufficiently high energy density, many aspects of this transition are still a matter of debate. Such "details" are, e.g., the order of the phase transition, the precise value of the critical energy density, the nature of experimentally observable signatures of the transition, and whether equilibrium conditions are established in nuclear collisions over a sufficiently large space-time volume. These questions require theoretical and experimental study. Here we will be concerned with theoretical aspects; for the experimental part the reader is referred to Prof. Otterlund's lecture at this

school. Finally, we will discuss some recent fascinating speculations about the possible use of peripheral heavy ion collisions at even higher energies (TeV/u) as a laboratory of electroweak physics at the unification scale.

2. PHYSICS OF THE QUARK-GLUON PLASMA

2.1. The QCD Phase Transition

Most aspects of the strong nuclear interaction are (at least) qualitatively explained by quantum chromodynamics (QCD), the gauge theory of color-SU(3). The two fundamental building blocks of this theory are the *quarks*, point-like fermions carrying baryon number 1/3 and transforming under the triplet representation, and the *gluons*, massless vector bosons forming an octet representation of the color gauge group. Under normal conditions only color singlet states have finite energy, hence quarks and gluons are confined into spatial regions approximately 1-2 fm in diameter. The precise mechanism for this confinement property of QCD is still unknown, but it is clear that asymptotic freedom, i.e. the fact that the strong coupling constant α_s decreases for high and increases for low momenta, is the underlying reason. Numerical solutions of the nonabelian gauge theory on a space-time lattice have shown that the potential between a static quark-antiquark pair has the form [4]

$$V(r) \longrightarrow \begin{cases} [r \ln(\Lambda r)]^{-1} & \text{for } r \rightarrow 0; \\ \kappa r + c & \text{for } r \rightarrow \infty. \end{cases} \quad (1)$$

κ is called the QCD string constant; from the slope of the hadronic Regge trajectories its value is known to be about 0.9 GeV/fm.

The fact that α_s becomes of order 1 at $r = 1$ fm has two consequences: (1) As already mentioned, color forces are effectively screened at this distance by the formation of color-singlet hadrons, i.e. by color confinement. [In full QCD with dynamical quarks the confinement question becomes quite subtle, since the quark-antiquark potential is screened due to the possibility of creating additional quark-antiquark pairs from the vacuum, which break the color flux tube between the original pair.] (2) It is known that massless fermions subject to a vector interaction acquire a dynamical mass through the breaking of chiral symmetry, when the coupling constant becomes of order 1 [5]. For quarks this dynamical mass term is of the order $m_q^{\text{eff}} \approx 300$ MeV. This term adds to the so-called "current" quark masses, which are generated by interaction with the electroweak Higgs field,

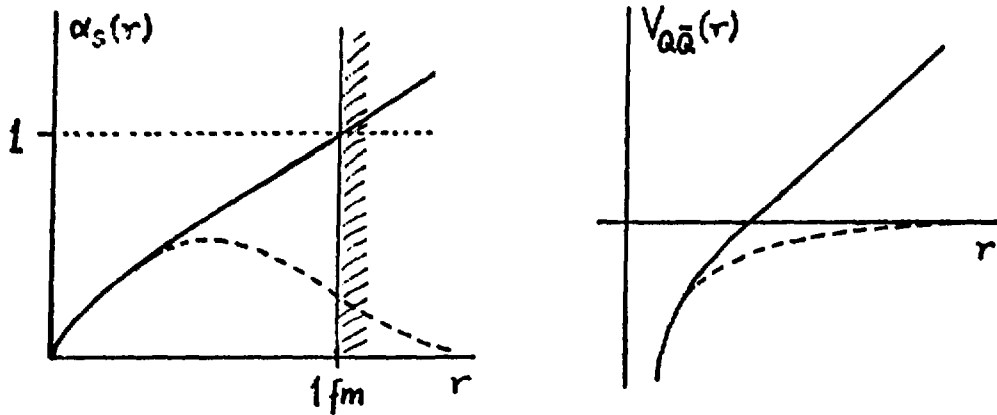


Fig. 1: Schematic plot of the radial dependence of the static quark-antiquark potential $V_{Q\bar{Q}}(r)$ and of the effective QCD coupling constant $\alpha_s(r)$ it in vacuo (solid lines) and in the presence of superdense QCD matter (dashed lines).

and are somewhat uncertain since they cannot be measured directly due to the confinement property. Broadly accepted values are $m_u = 5$ MeV, $m_d = 10$ MeV, and $m_s = 170$ MeV.

At sufficiently high quark or gluon density the picture changes completely. When the average separation between colored particle far exceeds 1 fm^{-3} , color screening can occur by the Debye mechanism, where a screening cloud of quarks and gluons form around each particle *inside* a sphere of 1 fm, thus preventing α_s ever to become large. The mechanism is illustrated in Fig. 1, where the changes in α_s and the quark-antiquark potential $V(r)$ are schematically shown. Taking the mean nucleon radius as 0.8 fm, the quark density in its interior is of order 1.4 fm^{-3} ; a radical change in the properties of QCD can thus be expected when nuclear matter is so much compressed that nucleons begin to overlap.

What happens then? The common belief among QCD theorists is that hadronic matter then goes over into a “plasma” of quasi-free quarks and gluons, that interact rather weakly through the screened color forces, no longer being confined to a region of about 1 fm in size. Simultaneously with deconfinement the dynamical quark masses should disappear, because α_s is no longer strong enough to sustain chiral symmetry breaking. If this picture were correct, the equation of state of QCD matter beyond the phase transition point could be approximately described as an ideal gas of relativistic particles, with corrections of order α_s due

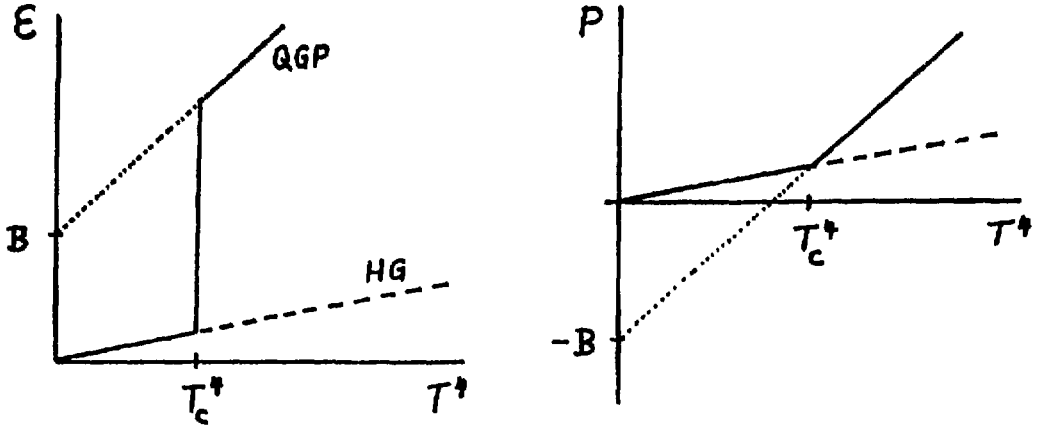


Fig. 2: Energy density (left) and pressure (right) as function of temperature for the equation of state (2).

to color interactions and terms arising from the change in the vacuum structure of QCD. An often assumed form of the equation of state of QCD matter in the hadronic and plasma phases (index 'h' or 'p', resp.) is:

$$\begin{aligned}
 \text{energy density :} \quad \epsilon_h &= g_h \frac{\pi^2}{30} T^4 & \epsilon_p &= g_p \frac{\pi^2}{30} T^4 + B \\
 \text{pressure :} \quad P_h &= g_h \frac{\pi^2}{90} T^4 & P_p &= g_p \frac{\pi^2}{90} T^4 - B, \quad (2)
 \end{aligned}$$

where the relevant numbers of degrees of freedom are $g_p = 37$ (2×8 for gluons and $2 \times 2 \times 3 \times \frac{7}{8}$ for u- and d- quarks) and $g_h = 3$ for an ultrarelativistic pion gas. The correct effective value for g_h may be considerably larger due to the excitation of hadron resonances. The vacuum term B (bag constant) is estimated to be of order $200 \text{ MeV}/\text{fm}^3$. As Fig. 2. illustrates, this equation of state predicts a phase transition at a critical temperature $T_c \approx 200 \text{ MeV}$. The critical energy density is somewhere between 2 and $4 \text{ GeV}/\text{fm}^3$.

This picture is supported by numerical simulations of lattice QCD. Results for the pure $SU(3)$ gauge theory without dynamical quarks are fairly good, predicting critical temperatures in the range between 200 - 250 MeV [6] depending which reference quantity is taken. [Lattice QCD only allows for the computation of dimensionless ratios, e.g. of T_c to the string constant, or some hadron mass.] A typical result is shown in Fig. 3a, where ϵ/T^4 is plotted as function of the temperature T . Numerical results for full QCD, i.e. $SU(3)$ gauge theory with light dynamical quarks, are less certain, but calculations also indicate the presence of a

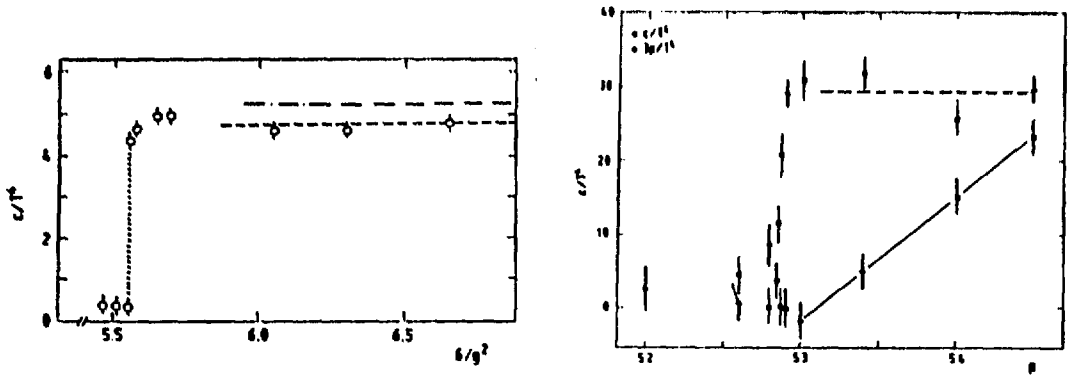


Fig. 3: (Left, a) ϵ/T^4 versus a lattice parameter measuring the effective temperature T for pure SU(3) gauge theory. (Right, b) Same for QCD with two light quark flavors [7]; P/T^4 is plotted in addition here. Lines are to guide the eye.

rapid phase change, where approximate chiral symmetry is restored and the effective number of degrees of freedom increases rapidly, if not discontinuously, with T (see Fig. 3b).

2.2. Signatures of the Quark-Gluon Plasma

2.2.1. *Overview:* According to the laws of general relativity, the entire universe was a giant quark-gluon plasma during the first few microseconds after the “big bang” when its temperature was in excess of 200 MeV. Few relics of this phase remain today, with the possible exception of some forms of “dark” matter and granularity that may have arisen as a consequence of density fluctuations generated during the phase transition to hadronic matter [8]. To study the properties of deconfined QCD matter we must thus rely on laboratory experiments involving central collisions of nuclei at energies sufficiently high to trigger compression of nuclear matter to the elevated energy density required for the phase transition. Since it is rather unlikely that quark matter, once created, will remain stable under any circumstances,¹ the task is to find signatures of the temporary presence of a quark-gluon plasma that survive its decay. Many signals have been suggested as characteristic signature; an incomplete list reads as follows [11]:

Lepton pairs (e^+e^- , μ^+ , μ^-)

Strange antibaryons ($\bar{\Lambda}$, $\bar{\Xi}$, etc.)

¹Quark matter with a high excess of strange quarks may be an exception. It is conceivable that such *strangelets* are sometimes formed in nuclear collisions [9,10], and experiments dedicated to their search are in progress at the Brookhaven AGS.

Antimatter (\bar{p} , \bar{d} , $\bar{\alpha}$)

Direct photons (not originating from π^0 - or η -decay)

Absence of charge correlations

Bend in $\langle p_T \rangle$ versus multiplicity density

Suppression of charmonium production

Quark jet acoplanarity

Multiplicity fluctuations

Even a quick look at this rather long list shows that there is no agreement as to what a really good signal is. To a large part this difficulty is due to the short expected lifetime of a quark-gluon plasma in nuclear collisions; a few fm/c hardly suffice to generate an unambiguous signal identifying the presence of a new state of QCD matter. Apart from fundamental aspects – [How large must the space-time volume be so that it becomes meaningful to speak of a phase transition?] – the problem comes from the large background contribution to all conceivable signals from the hadronic matter phase. In general, quark-gluon plasma signatures can be classified as follows:

1. Kinematic observables probing the existence of a phase change in the equation of state of QCD matter, but not the nature of the transition.
2. Penetrating (mostly electromagnetic) probes testing the increased density of charged particles (quarks) in the plasma phase.
3. Hadronic observables probing color deconfinement or chiral symmetry restoration in the high-temperature phase,

Kinematic signals: A characteristic example is the dependence of the average transverse momentum of emitted particles $\langle p_T \rangle$ versus multiplicity density dN/dy , where y is the rapidity. The idea here is that dN/dy is a measure of the violence of the collision and of the energy density ϵ reached, while $\langle p_T \rangle$ measures the temperature and pressure of the fireball. When ϵ is steadily increased from rather low levels, the mean p_T grows steadily. However, when one enters into the phase transition region, the temperature of the fireball remains constant while the energy density continues to grow due to conversion of an ever larger fraction of hadronic matter into quark-gluon plasma. The temperature increases again, when

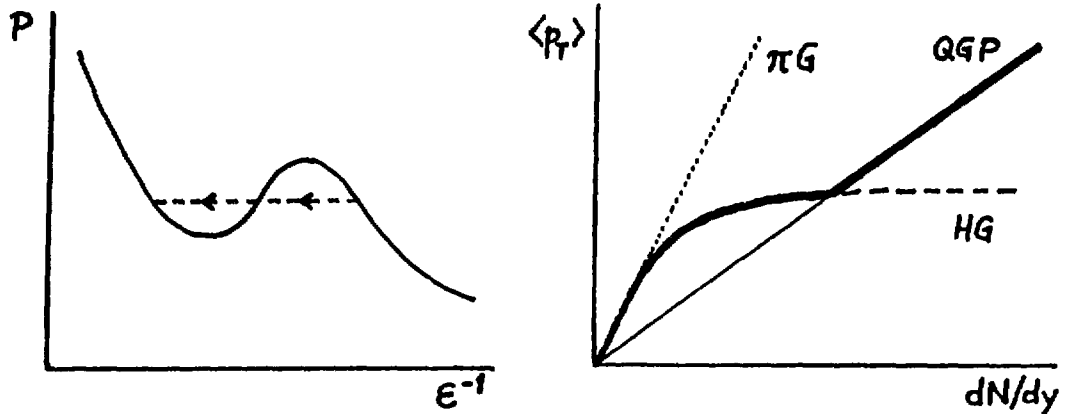


Fig. 4: (Left) Pressure versus energy density for an equation of state with a first order phase transition. (Right) Average p_T versus multiplicity dN/dy for a pion gas (dotted), Hagedorn gas (dashed), and a quark-gluon plasma (solid line). The thick solid line indicates the path taken in the presence of the phase transition.

the full latent heat of the transition is provided. One thus expects that the relation between $\langle p_T \rangle$ and dN/dy exhibits a flat region at intermediate values and continues to rise at higher values of dN/dy [12,13]. By comparison, a Hagedorn gas with limiting temperature would remain flat forever (see Fig. 4).

Electromagnetic signals: The most widely discussed of these is the invariant mass spectrum of lepton pairs [14,15]. Here the contribution from a quark-gluon plasma is predicted to fill in the intermediate range between the mass of the ρ -meson, which dominates hadronic lepton-pair production, and the high-energy tail due to Drell-Yan pairs created in the initial part of the collision, when the participating nucleon still have their full energy. The disappearance of the characteristic ρ -meson peak under certain conditions, e.g. high transverse momentum of the lepton pair, would signal the existence of a long-lived non-hadronic phase during the collision.

Hadronic probes of deconfinement: While these signals are, in principle, the most sensitive and interesting ones, they have two important disadvantages: (a) strongly interacting probes are hard to predict quantitatively; (b) hadronic processes always compete. The two most widely studied signals are the enhanced production of strange hadrons and the suppression of charmonium production. Because of their special interest, let us now discuss these two in more detail.

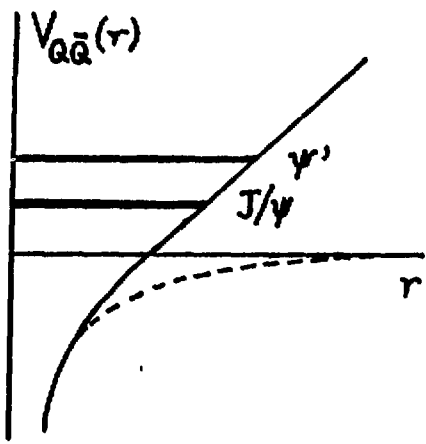


Fig. 5: (Left) Screening of the $Q\bar{Q}$ potential leads to the disappearance of charmonium bound states in the quark-gluon plasma.

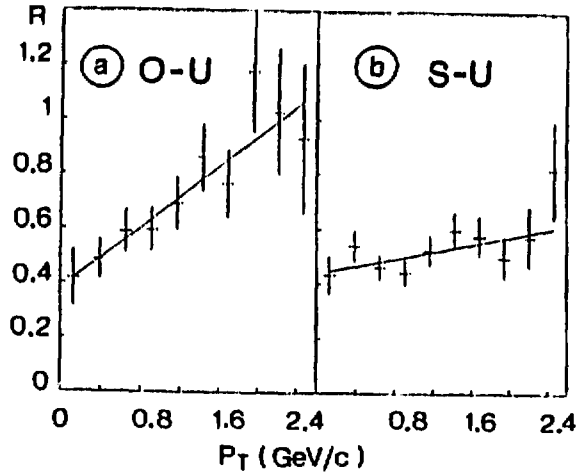


Fig. 6: (Right) Observed suppression of J/ψ in central O+U and S+U collisions (data: NA38).

2.2.2. Charmonium suppression: Due to their large mass charmed quarks are almost exclusively produced in the initial collisions among nucleons of the two heavy ions by two-gluon scattering. For the production of a J/ψ charmonium state this process must be followed by emission of a soft gluon to get into the spin-1 channel. Now, if the produced $c\bar{c}$ pair finds itself in an environment where the quark-antiquark potential is Debye-screened at a distance of, say, 0.4 fm it will not be able to form a J/ψ because the screened potential does not support a bound state [16], as illustrated in Fig. 5. [The radius of a J/ψ in free space is about 0.5 fm.] Does this imply that no J/ψ 's are produced if a quark-gluon plasma is formed? The answer is no, because the formation of a charmonium bound state takes some time, corresponding roughly to the period of oscillation of the $c\bar{c}$ pair in the J/ψ . If the $c\bar{c}$ pair has a high transverse momentum, it can escape from the region of space where deconfinement has occurred and then form a J/ψ . The suppression hence acts mainly at low transverse momentum of the J/ψ .

Such a pattern of suppression of J/ψ particles has in fact been observed in an experiment with 200 GeV/u oxygen and sulphur nuclei on heavy targets [17] (see Fig. 6). Unfortunately, careful theoretical studies have revealed that very efficient mechanisms for the destruction of J/ψ particles also exists in a purely

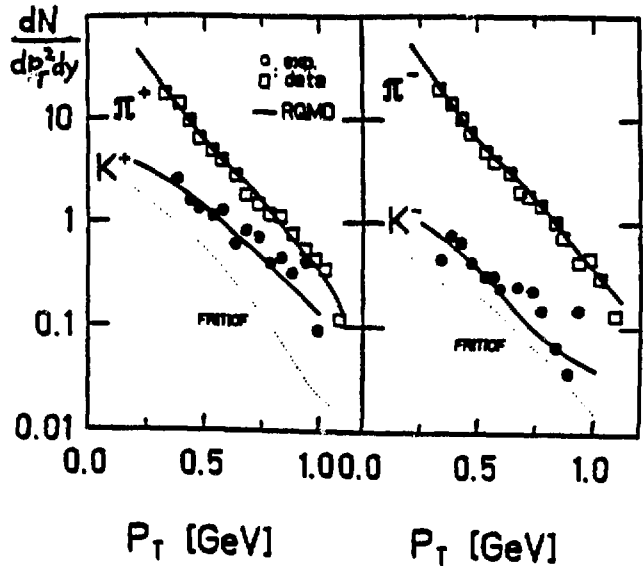
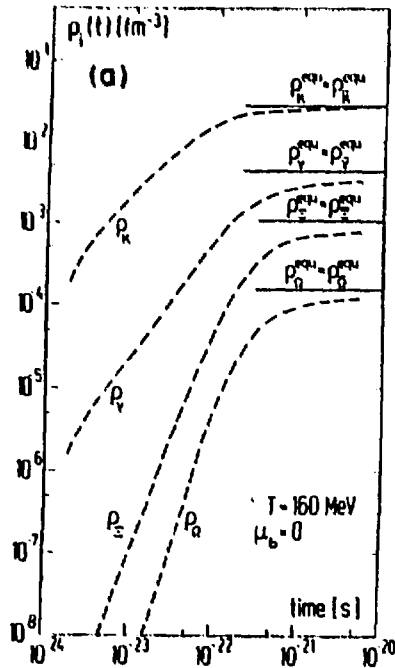


Fig. 7: (Left) The characteristic time-scale for approach to the equilibrium abundance of strange hadrons in hot hadronic matter is of the order of at least 10^{-22} s.

Fig. 9: (Right) The enhanced production of K^\pm mesons relative to charged pions observed in the E802 data is reproduced by relativistic cascade calculations, without assuming formation of a quark-gluon plasma.

hadronic environment which contains a large number of pions or ρ -mesons. Moreover, transverse momentum distribution of $c\bar{c}$ pairs in nuclear collisions is slightly tilted to higher momenta due to soft collisions before $c\bar{c}$ creation occurs. These two effects conspire to yield a picture that is virtually indistinguishable from that predicted in the case of quark-gluon plasma production, at least for the presently available experimental data [18,19].

2.2.3. Strangeness enhancement: An enhancement of strange particle production in a quark-gluon plasma environment was originally predicted for two reasons: (a) $s\bar{s}$ pairs are created mainly by gluon-gluon interactions [20], which are more abundant, and (b) $s\bar{s}$ pairs are more easily produced due to chiral symmetry restoration, which lowers the mass of a strange quark. This effect reduces the threshold for strangeness production from about 700 MeV in a hadron gas to about 350 MeV

in the plasma; a crucial difference in an environment characterized by a temperature of the order of 200 MeV. Moreover, the density of strange quarks would be about three times higher in the plasma than in the hadronic phase, so that hadrons with multiple strangeness content (Ξ , $\bar{\Xi}$, etc.) would be produced more easily. Extensive simulations of the kinetics of strangeness production in quark-gluon plasma and in hadronic matter support this picture [21]: multiple strange baryons or strange antibaryons are not produced as abundantly in a hot hadronic fireball as they would be in a quark-gluon plasma (see Fig. 7).

Again, experiments (E802 at Brookhaven, NA35 at CERN) which showed an enhanced level of strange hadron production in nuclear collisions, as compared with single nucleon collisions, appeared to confirm these ideas and to signal the formation of a QCD plasma. In particular, a strong increase in Λ production with charged particle multiplicity was observed in $^{32}\text{S}+\text{S}$ collisions at 200 GeV/u, which could not be explained by hadronic interaction in a thermal fireball (see Fig. 8). However, a recent theoretical study of the hadronic cascade leading from the initial state of two colliding nuclei to the expanding fireball has shown that preequilibrium processes may contribute decisively to K-meson and Λ production [24]. The K/π enhancement observed by experiment E802 can be fully explained in this way without the need to assume the formation of a quark-gluon plasma (see Fig. 9).

Summarizing this section, we can say that several signals for QCD plasma formation have been observed in recent experiments, but more refined theoretical studies have shown that these are not unambiguous signatures. This is no reason for despair, rather a stimulus for further work. At present we do not have a theoretical description of the nuclear collisions that would allow to treat the hadronic and the QCD plasma phase on the same level. It is quite possible that promising signatures will emerge when such models become available.

3. STRING MODEL OF HOT HADRONIC MATTER

3.1. Hadronic Strings

At the end of the previous section the need for a complete description of the nuclear collision dynamics became obvious. The ideal model for this should allow us to describe the nuclear matter of the incident nuclei on the same footing as the highly excited hadronic gas of the fireball in its later stage, as well as possibly

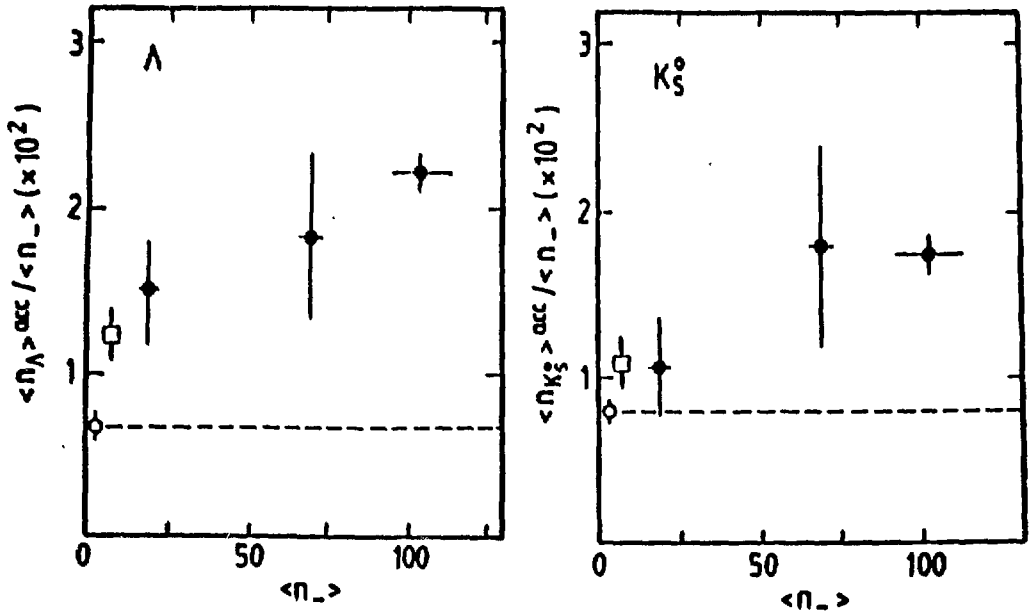


Fig. 8: Increase in the relative abundance of Λ and K_S^0 compared to all negatively charged hadrons versus multiplicity (n_{-}) (data: NA35).

an intermediate QCD plasma phase. At present, we do not have such a model. Here I would like to discuss one model that has been applied successfully to several, though not all, aspects of the nuclear collision: the hadronic string model. Let me first put this into perspective by reminding you of its origins (for more details see [25]).

About two decades ago Hagedorn [26] found that highly excited hadronic matter could be surprisingly well described as a *resonance gas* of noninteracting relativistic particles with a mass spectrum of the form

$$\rho(m) \propto m^{-a} \exp(m/T_0). \quad (3)$$

The slope parameter T_0 plays the role of a *limiting temperature*, because the energy density of such a gas in thermal equilibrium scales as $\epsilon(T) \propto (T_0 - T)^{-\nu}$, hence T can never exceed T_0 . (It was later pointed out that the gas exhibits a singularity at finite energy density if an excluded volume correction for the finite size of hadrons is applied [27].)

At this point the question emerges immediately, as to how a noninteracting resonance gas can come into thermal equilibrium. Obviously there is a need for

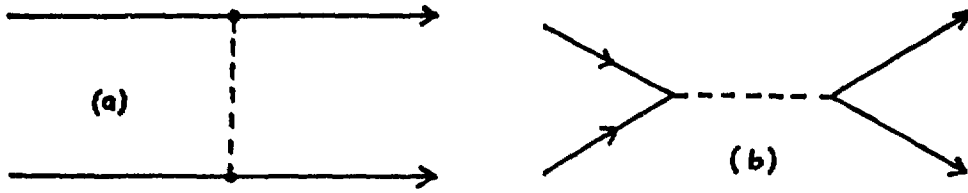


Fig. 10: Hadron scattering with t -channel exchange (a: left) and s -channel exchange (b: right) of a virtual meson.

interactions and an underlying dynamics that explains the peculiar form of the mass spectrum (3). The first step in this direction was the *dual resonance model* of Veneziano [28]. It was based on the observation that the scattering amplitudes for two hadrons exchanging a meson of angular momentum J_n and mass M_n in the t -channel (see Fig. 10a)

$$A_n(s, t) = g_n^2 (-s)^{J_n} [M_n^2 - t]^{-1} \quad (4)$$

had a most undesirable dependence on total energy s , if $J_n > 0$, and there are many mesons known with $J_n = 1, 2, \dots, 6$. On the other hand, total cross sections are known to rise at most logarithmically with s due to unitarity (Froissart bound). The dilemma may be resolved, if the many contributions from different mesons combine into the Taylor series of a much better behaved function of s . [In a similar way as the terms $\frac{(-x)^n}{n!}$ yield the well-behaved function e^{-x} .] Veneziano suggested that the total amplitude obtained as sum of $A_n(s, t)$ over all mesons should equal the sum obtained from the s -channel scattering diagrams (see Fig. 10b)

$$A'_n(s, t) = g_n^2 (-t)^{J_n} [M_n^2 - s]^{-1}, \quad (5)$$

which is well-behaved in the variable s .

This equivalence between s - and t -channel diagrams can indeed be achieved, if the meson masses are arranged according to the pattern

$$M_n^2 = [J_n - \alpha(0)]/\alpha', \quad (6)$$

where $\alpha(0)$ and α' are constants to be taken from experiment. As you know, this relation is quite well satisfied in nature; mesons of the same flavor quantum number but different spin fall on linear Regge trajectories with $\alpha' \approx 1\text{GeV}^{-2}$. A simple hadronic model which yields this type of excitation spectrum is the relativistic

string model, idealizing an (excited) hadron as an infinitely thin, massless string with tension

$$\kappa = (2\pi\alpha')^{-1} \approx 0.89\text{GeV/fm}. \quad (7)$$

The Veneziano formula is naturally obtained as the scattering amplitude of relativistic strings on the tree level [29].

Unfortunately, there is the problem that a consistent quantum theory of the relativistic string is known only in (25+1) space-time dimensions, where the longitudinal modes decouple from the string dynamics. In the (3+1)-dimensional Minkowski space, strings can only be the basis of an effective, semiclassical theory of hadrons. However, this makes sense as long as we consider only interactions among strings at the tree level and no loop diagrams, where the full quantum mechanics becomes important. Indeed, there are many indications that string-like excitations occur naturally in QCD, for example:

1. The quark-antiquark potential rises linearly with distance, as evidenced by simulations of the SU(3) lattice gauge theory and potential model fits to the charmonium and Upsilon spectra.
2. In the framework of the MIT bag model configurations corresponding to widely separated quarks exhibit a string-like shape, with a color flux-tube forming between the quarks. A bag constant of $B^{1/4} = 190 \text{ MeV}$, and $\alpha_s = 1$ correspond to a string tension of 1 GeV/fm.
3. Lattice simulations of the color fields extending between a quark-antiquark pair show that the field energy is concentrated along the line connecting the quarks, with a transverse extension of about 0.3–0.4 fm [30].

In fact, string-like excitations may dominate many high-energy phenomena involving QCD, such as hadron jet production observed in electron-positron annihilation, and multiparticle production in proton-proton collisions at high energy. Phenomenological models based on the string picture, such as the Lund model, have been very successful at describing the global properties of such events, and are widely used in the analysis of experimental data.

These phenomenological models usually combine aspects of the string picture, especially those of longitudinal string excitations, with other heuristic as-

sumptions, e.g. with respect to the transverse momentum distribution of created particles. This introduces a certain amount of arbitrariness into the models, which makes it hard to apply them to novel situations, and also leaves questions as to their internal consistency. It is therefore of interest to explore how far the *pure* hadronic string model is able to describe the dynamics of highly excited hadronic states, from hadron jets to thermally equilibrated, hot hadronic matter. Note that the model contains only two dimensional parameters:

1. The string constant, $\kappa = 0.89 \text{ GeV/fm}$, from the experimental Regge slope.
2. A finite string or flux-tube radius of $R = 0.5 \pm 0.1 \text{ fm}$, consistent with the lattice QCD results.

We shall see that this model, although essentially parameter-free, describes many aspects of high-energy hadron dynamics surprisingly well.

3.2. Free String Motion

The motion of a massive relativistic point particle is described by a *world line* $x^\mu(\tau)$, where τ is the proper time measured along the world line. The world line is governed by the action

$$S = -mc \int d\tau = -mc \int (\dot{x}^\mu \dot{x}_\mu)^{1/2} d\tau, \quad (8)$$

yielding the equation of motion $d^2x^\mu/d\tau^2 = 0$, i.e. the world line is a straight line in Minkowski space. The free relativistic string is obtained by the generalization to a one-dimensional object of finite length, corresponding to a contiguous set of (massless) point particles arranged along a (not necessarily straight) line. Here we will consider only *open* strings, where the left and right endpoints do not coincide. Moreover, we will assume – where necessary – that the strings are *oriented*, one end corresponding to the position of a QCD charge of the fundamental triplet representation, the other end to that of a QCD charge of the antitriplet representation of color-SU(3). The one may be thought of as a valence quark, the other as an antiquark or, in the case of baryons, as a diquark (see Fig. 11). The string itself is supposed to be an idealization of the color flux-tube extending between the spatially separated color charges.

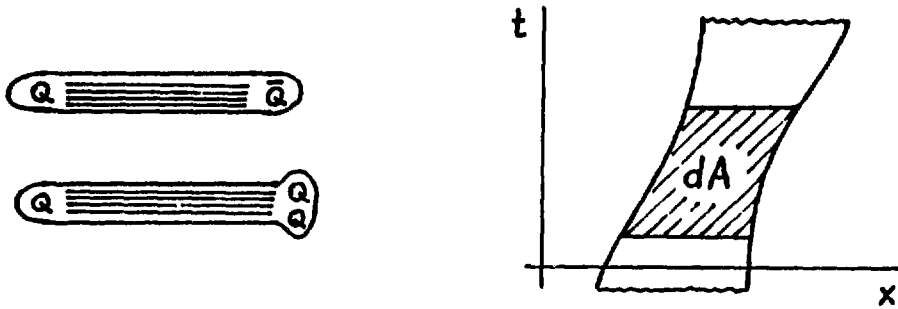


Fig. 11: (Left) Meson and baryon strings are oriented flux-tubes.

Fig. 12: (Right) World sheet of the relativistic string. The world line of the left endpoint is also called the *directrix*. It determines the motion of the entire string.

On its motion through Minkowski space, the string sweeps out a two-dimensional surface, called the *world sheet*, parametrized in the form $x^\mu(\sigma, \tau)$, where the space-like parameter measures the points along the string (see Fig. 12). The Nambu-Goto action governing the motion of the free string is given by the invariant area of the world sheet, namely:

$$S = -\kappa \int dA = -\kappa \int d\sigma d\tau [(\dot{x} \cdot x')^2 - \dot{x}^2 x'^2]^{1/2}, \quad (9)$$

where the “dot” denotes a derivative with respect to τ and the “prime” a derivative with respect to σ , and $(a \cdot b)$ denotes a four-dimensional scalar product. The action (9) is invariant against reparametrizations $(\sigma, \tau) \rightarrow (\sigma', \tau')$, which has similar consequences as gauge invariance in gauge theories. Its pleasant aspect is that we may choose a convenient set of parameters, e.g. identify τ with the reference frame time coordinate: $\tau = x^0 = t$, and take σ proportional to the energy density carried by the string, i.e. $0 \leq \sigma \leq E/\kappa$, where E is the total energy of the string in the chosen frame of reference. The equation of motion derived from the Nambu-Goto action is then:

$$\partial^2 \vec{x} / \partial t^2 - \partial^2 \vec{x} / \partial \sigma^2 = 0, \quad (10)$$

with the boundary conditions

$$\vec{x}'(t, 0) = \vec{x}'(t, E/\kappa) = 0. \quad (11)$$

Due to the reparametrization invariance, these equations are supplemented by two nonlinear constraint equations, viz.

$$\frac{\partial \vec{x}}{\partial t} \cdot \frac{\partial \vec{x}}{\partial \sigma} = 0, \quad \left(\frac{\partial \vec{x}}{\partial t}\right)^2 + \left(\frac{\partial \vec{x}}{\partial \sigma}\right)^2 = 1. \quad (12)$$

It is the presence of these two constraints, which makes the quantization of string theory so difficult.

There are basically two ways of solving the system of equations (10-12). The first one, which is an appropriate route to the quantum theory of strings, is based on the Fourier series expansion of the most general solution of the two-dimensional wave equation (10) under the boundary conditions (11), which is given by:

$$\vec{x}(t, \sigma) = \vec{X}_0 + \frac{\vec{P}}{E}t + \frac{E}{\pi\kappa} \sum_{n \neq 0} \frac{1}{n} \vec{\alpha}_n e^{-int} \cos(n\pi \frac{\kappa}{E}\sigma). \quad (13)$$

In order to fulfill the nonlinear constraint equations (12), the Fourier coefficients $\vec{\alpha}_n$ must satisfy the so-called *Virasoro* conditions

$$L_m \equiv 1 - \sum_n \vec{\alpha}_{m-n} \cdot \vec{\alpha}_n = 0, \quad (14)$$

where $\vec{\alpha}_0 = \vec{P}/E$ is the center of mass velocity of the string. Although useful for the formal analysis of string theory, this representation of the solutions of the equation of motion is not very practical for numerical simulations due to the nonlinearity of the Virasoro conditions (14).

The second approach is based on the observation that the most general solution of the wave equation (10) is a superposition of an arbitrary wave front moving to the left and one moving to the right:

$$\vec{x}(t, \sigma) = \frac{1}{2}[\vec{y}(t + \sigma) + \vec{y}(t - \sigma)]. \quad (15)$$

The left- and the right-moving front must be the same because the string is open and the wave fronts are reflected at the ends of the string. Inserting $\sigma = 0$ one finds the meaning of the function $\vec{y}(t) = \vec{x}(t, 0)$; it describes the trajectory of the left endpoint of the string, or the *directrix*. In other words, the motion of the entire string is completely determined by that of one of its endpoints! Because the momentum density carried by the string is given by

$$\vec{\Pi}(t, \sigma) = \frac{1}{2}[\vec{y}(t + \sigma) - \vec{y}(t - \sigma)], \quad (16)$$

the boundary condition (11) stipulates that the directrix must be periodic, except for a constant shift in the direction of the total momentum:

$$\vec{y}(t + 2E/\kappa) = \vec{y}(t) + 2\vec{P}/\kappa. \quad (17)$$

The nonlinear constraints (12) reduce to a single equation:

$$(d\vec{y}(t)/dt)^2 = 1, \quad (18)$$

showing that the endpoint always propagates with the speed of light. This is, of course, due to the assumption that the endpoints – as all other points on the string – do not carry a rest mass. So all one has to do to obtain a valid solution of the equations of motion of the free string is to construct an arbitrary curve $\vec{y}(t)$ with a unit gradient vector. To generate an ensemble of such curves is a simple numerical problem (see e.g. [25]). Simple and well-known solutions of the equation of motion are:

1. Straight-line strings performing strictly longitudinal oscillations. These solutions are often termed “yoyos”; they form the basis of most string models for high-energy particle collisions (see Fig. 13a)
2. Rigidly rotating rod-like strings. These modes have the lowest mass m for given angular momentum J , satisfying the linear Regge trajectory relation $m^2 = 2\pi\kappa J$ (see Fig. 13b).
3. General solutions can be constructed numerically by specifying discrete points on the directrix, and connecting them by (light-like) straight segments. The resulting string can then easily be traced along its motion in Minkowski space (see Fig. 14 for an example).

One can now construct a representative microcanonical ensemble of the possible string modes for a given total energy E . Their c.m. momentum \vec{P} can be directly read off the directrix using eq. (17), so that the mass spectrum $\rho(m)$ of strings with mass $m < E$ is easily obtained by numerical simulation [30]. The result is shown in Fig. 15 together with the asymptotic formula

$$\rho(m) \rightarrow \frac{\kappa^{3/4}}{(4\pi)^{1/4}} m^{-5/2} \exp\left(\frac{m}{T_0} + \frac{1}{2}\right), \quad (19)$$

where $T_0 = \pi^{1/6}\kappa^{1/2}/2 \approx 250$ MeV is the limiting temperature. For small masses the exact mass distribution differs substantially from the asymptotic expression, in particular, its slope stays positive everywhere.

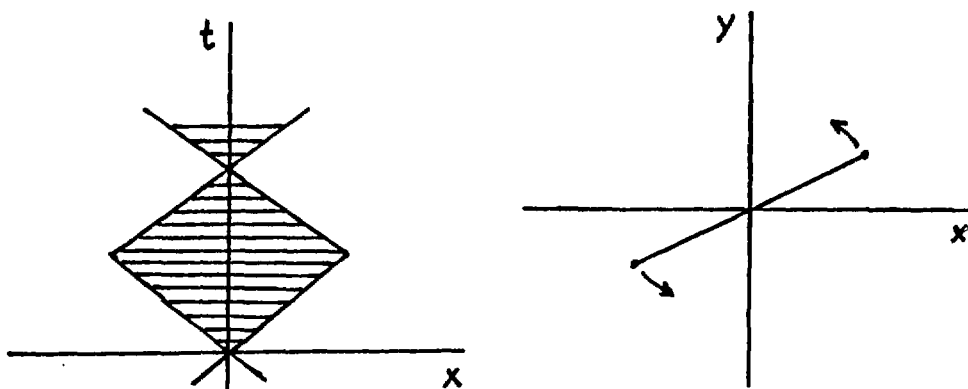


Fig. 13: Simple string modes are the longitudinal oscillation, the so-called “yoyo” (a: left) and the rigidly rotating rod (b: right), which yields the leading Regge trajectory.

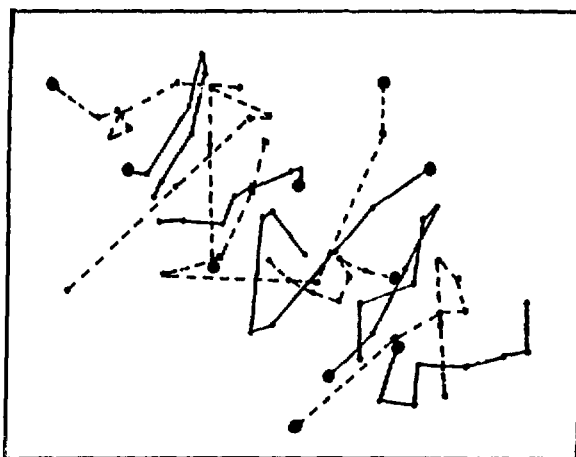


Fig. 14: Random motion of a string, constructed from its directrix. The picture shows consecutive snapshots of the string configuration projected onto a plane. The dark dot indicates the position of the left endpoint.

It is interesting to observe that the slope is in good agreement with that of the smoothed experimental hadron spectrum (shown by the solid line) below about 1.3 GeV; for higher masses the experimental spectrum probably is incomplete. The difference in normalization can be explained by the additional spin-flavor multiplicity of hadron states not accounted for by the simple string model: Counting the possible combinations of spin and flavor of the valence quarks at the endpoints of the string one finds a total number of $(36 + 56)$ for mesons and baryons, which puts the theoretical $\rho(m)$ right on top of the experimental hadron mass spectrum!

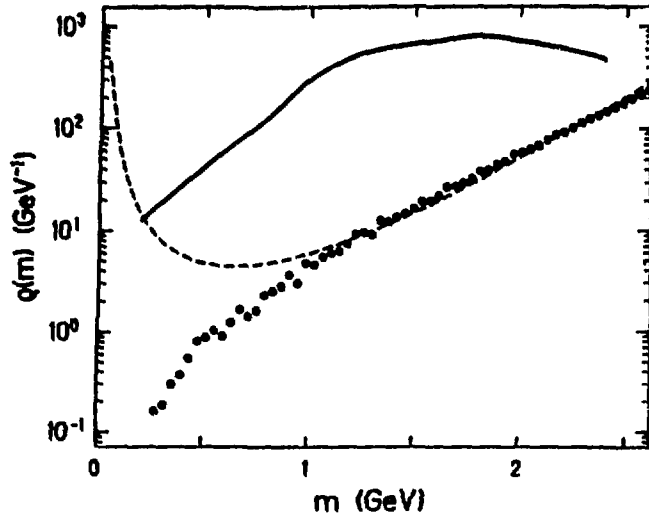


Fig. 15: Mass spectrum of the relativistic string. Dots: numerical simulation; dashed curve: asymptotic formula (19); full line: smoothed experimental mass spectrum.

It is just as easy to generate a canonical ensemble of strings at fixed temperature, which can be compared with the prediction of the Hagedorn model with the same limiting temperature. Fig. 16 shows how the mass distribution of hadrons in a free string gas for various temperatures; the increase in the abundance of heavier hadrons is conspicuous.

3.3. String Decay

Strings can interact in two fundamental ways: they can decay by splitting into two pieces, and two strings can exchange “arms” when they encounter. Let us first consider here the string decay, which corresponds to a simple “cut” in the world sheet of the string (Fig. 17). Just as the probability for decay of an unstable point particle is proportional to the (infinitesimal) proper time along its world line, $dP = \lambda d\tau$, the differential decay probability of a string is proportional to the invariant area swept out by its world sheet:

$$dP = \gamma dA = \gamma dL d\tau, \tag{20}$$

where dL is the length element in the local rest frame of the string. The decay constant γ must be universally proportional to the string constant κ , as can be shown by general arguments [31].

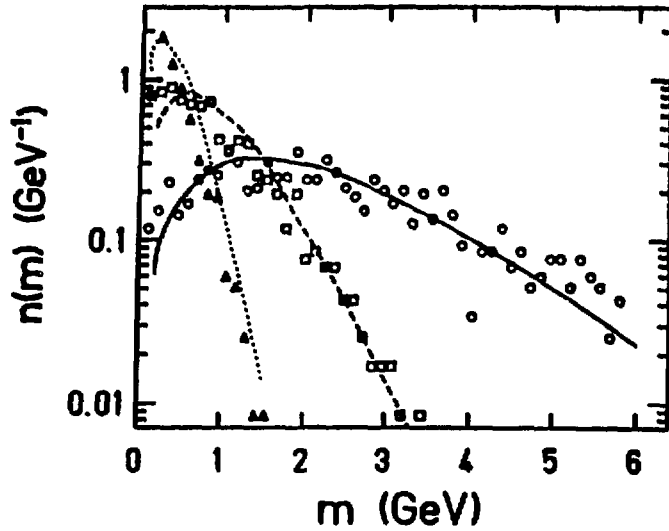


Fig. 16: Comparison of the simulated rest mass distributions $\rho(m)$ of strings with the theoretical ones (smooth curves) for the ideal string gas with temperature $T = 100$ MeV (triangles), 150 MeV (squares), and 200 MeV (circles).

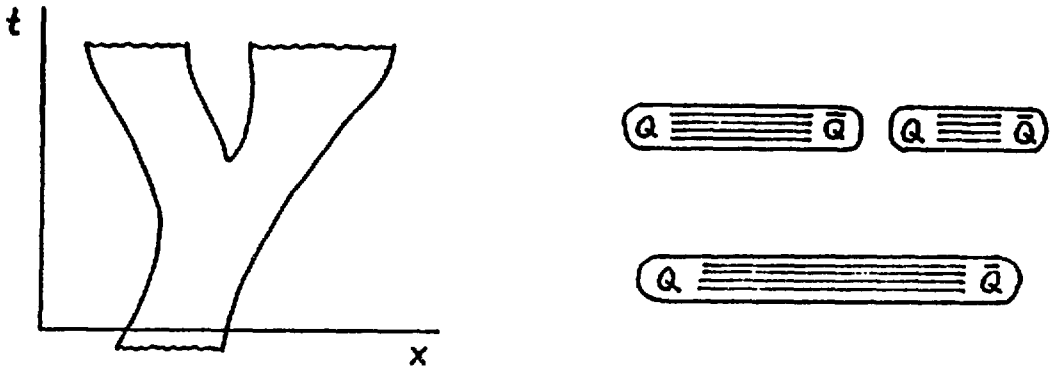


Fig. 17: (Left) Decay of a string corresponds to a timelike split in its world sheet.

Fig. 18: (Right) Decay of a flux-tube by spontaneous creation of a quark-antiquark pair.

Its precise value can be derived in a version of the flux-tube model [32]. Picture the string as a color flux tube of finite radius R and very large length, with color triplet charges at its ends. It will break as a consequence of spontaneous quark pair production somewhere along its line in the constant color-electric field that forms the flux tube (see Fig. 18). For the states of the new created quarks we take eigenstates of the Dirac equation in a constant background field of strength

\mathcal{E} with MIT-bag boundary conditions at the radial edge of the flux tube:

$$[\gamma^\mu(p_\mu - g\mathcal{A}_\mu) - m]\psi = 0, \quad \mathcal{A}_\mu = (\vec{0}, \mathcal{E}t), \quad (21)$$

$$(1 - i\gamma^\mu n_\mu)\psi|_R = 0. \quad (22)$$

The states are characterized by quantum numbers n, μ, p , where μ is the orbital angular momentum around the tube axis, p the momentum along the axis, and n enumerates the solutions of the transcendental equation (for $m = 0$)

$$J_{\mu+1}^2(x_{n\mu}) = J_\mu^2(x_{n\mu}), \quad (23)$$

with lowest values $x_{10} = 1.435, x_{11} = 2.63, x_{20} = 3.11$, etc. When these states are analyzed according to their asymptotic particle, resp. antiparticle content, one finds that the total rate of pair creation per unit length and time interval is given by [32]

$$dP = \frac{g\mathcal{E}}{\pi} \sum_{n,\mu} \ln\left[1 - \exp\left(-\frac{\pi x_{n\mu}^2}{g\mathcal{E}R^2}\right)\right] dL d\tau. \quad (24)$$

When one also applies the MIT bag model to the color field in the flux tube, one finds that $g\mathcal{E} = \kappa$. So indeed, dP is proportional to κ , with a constant that depends on the flux tube radius R .

Of particular interest is the transverse momentum distribution of the produced quark pairs, because it determines the experimental transverse momentum spectrum of hadrons formed in the decay of a highly excited color string. Good data for this are available from observations of quark jets in e^+e^- collisions, but they do not agree with the distribution of the form $\exp(-\pi p_T^2/g\mathcal{E})$ predicted from the decay of an infinitely thick flux tube ("Schwinger model"). The experimental distributions of p_T are much too wide, and the phenomenological models have mostly used the width of the distribution as a fit parameter. The situation is entirely different, if we take the finite radius seriously, since then the p_T distribution of the pairs will be determined by the transverse Fourier transform of the solutions $\psi_{n\mu}(x)$, which is a function of the dimensionless variable $q_T = p_T R$:

$$dP_{n\mu} \propto \frac{x_{n\mu}^2}{(x_{n\mu}^2 - q_T^2)^2} \left([x_{n\mu} J_{\mu+1}(x_{n\mu}) J_\mu(q_T) - q_T J_\mu(x_{n\mu}) J_{\mu+1}(q_T)]^2 + [q_T J_{\mu+1}(x_{n\mu}) J_\mu(q_T) - x_{n\mu} J_\mu(x_{n\mu}) J_{\mu+1}(q_T)]^2 \right). \quad (25)$$

Good agreement with the p_T -distributions observed in quark jet fragmentation is obtained for $R \approx 0.5$ fm, as evidenced in Fig. 19c.

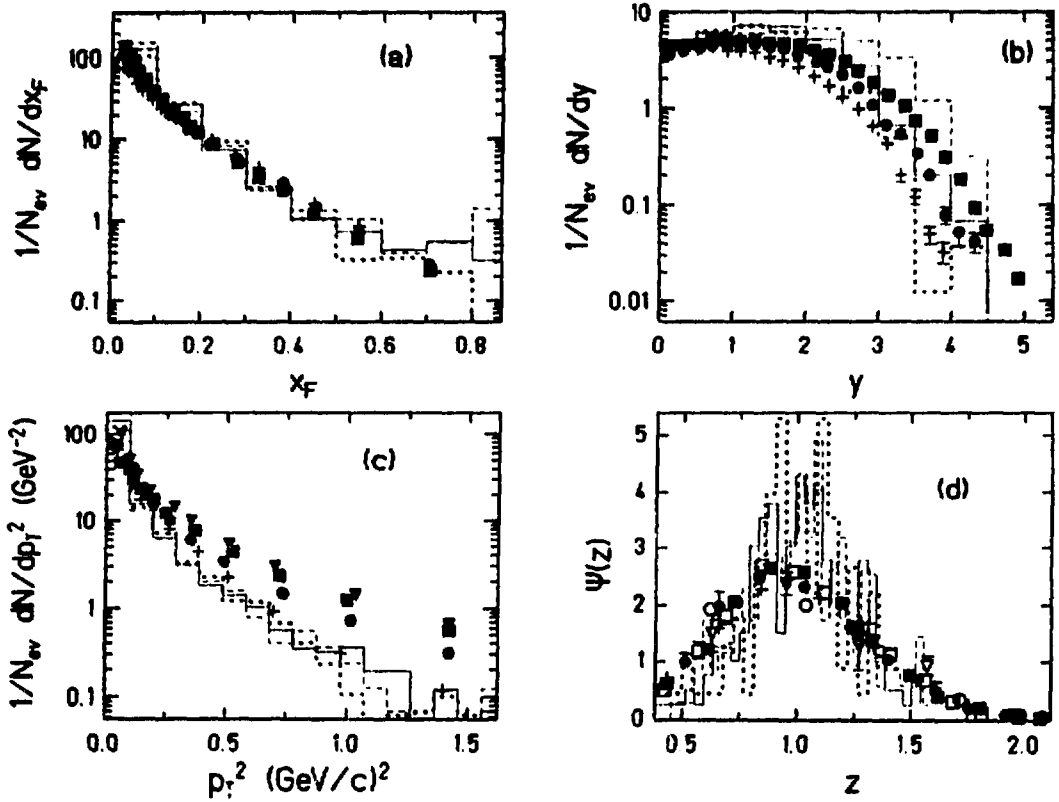


Fig. 19: Simulated (a) Feynman- x (x_F), (b) rapidity (y), and (c) transverse momentum (p_T) distributions of the fragments, as well as (d) KNO scaling functions $\psi(z)$ in e^+e^- annihilation compared to experimental data [Mättig et al., Phys. Rep. 177, 141 (1989)].

As the other parts of the figure show, the Feynman- x , rapidity, and multiplicity distributions are also well described, in particular, the latter exhibit KNO scaling in the variable $z = n/\langle n \rangle$. The remaining underestimate of the high- p_T tail of the spectrum has its origin in the distribution of the leading hadrons, which are experimentally broader than those in the central rapidity region, probably due to (soft) gluon bremsstrahlung. This process is missing in the semiclassical string picture. It has been accounted for in the Lund model in a very *ad hoc* manner by allowing for spontaneous formations of kinks along the string.

3.4. Interactions among String

In order to describe the dynamics of nucleus-nucleus collisions it is important to know how to treat interactions among strings correctly. At the semiclassical

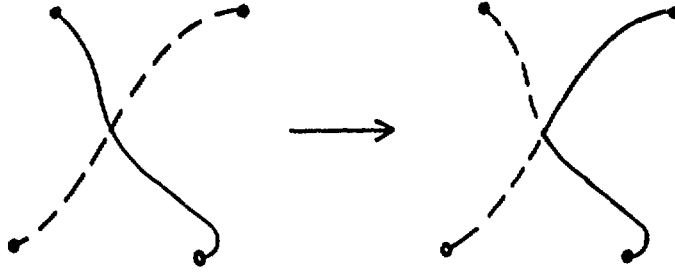


Fig. 20: Rearrangement interaction between two oriented strings which exchange their ends.

In order to describe the dynamics of nucleus-nucleus collisions it is important to know how to treat interactions among strings correctly. At the semiclassical level, two strings interact by exchanging their ends when they collide at some point (Fig. 20). Since our strings are oriented, this exchange can occur only in one way preserving the color-flux, or not at all. This raises the question as to the probability of rearrangement, which cannot be determined from the classical theory. In principle it could be calculated in a quantum theory of strings, if this existed in four dimensions, but then there would also be other interactions, e.g. by virtual exchange of strings. Computer simulations of collisions between classical, string-like vortex solutions of the abelian Higgs model have indicated that the probability of rearrangement is close to one, but this could be different for color-SU(3), and there could be a strong energy dependence. In our simulations we have assumed that two strings *always* exchange ends in an encounter.

If one models nucleons as strings of length about 1 fm, one finds that the (geometric) cross section for exchange is only a few millibarn, compared to the approximately constant experimental cross section at high energy of about 40 mb. This is a great disappointment, since the string model naively appears to provide a natural explanation of the roughly constant cross section. Two different resolutions of this problem have been explored:

1. Remler has suggested to artificially lower the string tension to increase its length and thus the geometric size of the nucleon [34]. Then κ must be reduced by a factor 4-5 to get the correct nucleon cross section of 40 mb.
2. Sailer et al. have allowed for a finite transverse extension of the string, which increases its geometric cross section [25]. Fig. 21 shows that a string radius

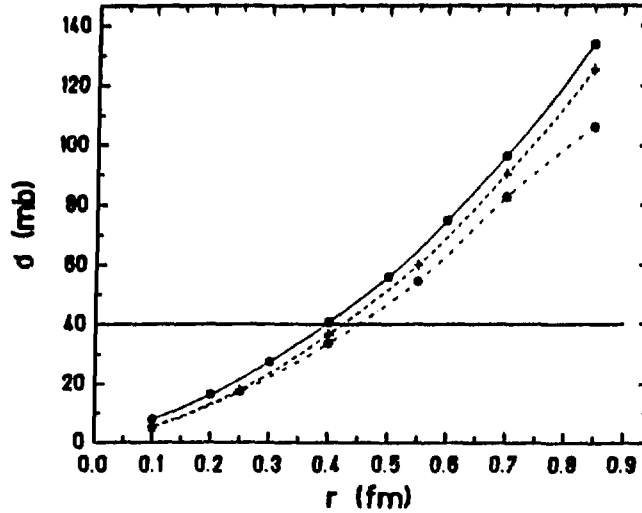


Fig. 21: Simulated total cross section of string-string collision vs. the string radius for various excitation modes: rotating rod (dots), yo-yo (crosses), and mixture of arbitrary modes (asterisks). The mass of the strings is taken to be the proton mass.

of 0.4 – 0.45 fm reproduces the experimental nucleon-nucleon cross section, independent of the string mode representing the nucleon.

In view of our previous discussion of string decay the second alternative appears more physical; a decrease in the value of κ would narrow the p_T -distribution even further. Moreover, the values of R obtained from the two considerations (p_T -spectra, N-N cross section) agree quite nicely. However, two unresolved questions remain in this approach: (1) The formal *Lorentz invariance* of string theory is lost when a finite radius of interaction is introduced. This is obvious when one considers that the apparent string radius depends on the reference frame of the observer. Although this may be resolved in an *ad hoc* manner by measuring the spatial distance between two strings in the local c.m. frame of adjacent string pieces, which are going to interact, it is not clear that such a recipe can be justified on the basis of more fundamental arguments. (2) The transverse momenta produced in collisions between two nucleon strings of finite thickness are still considerably too small when compared with experiment. A possible resolution of this problem is to allow for local momentum exchange between the strings during the finite time they are in direct contact [35].

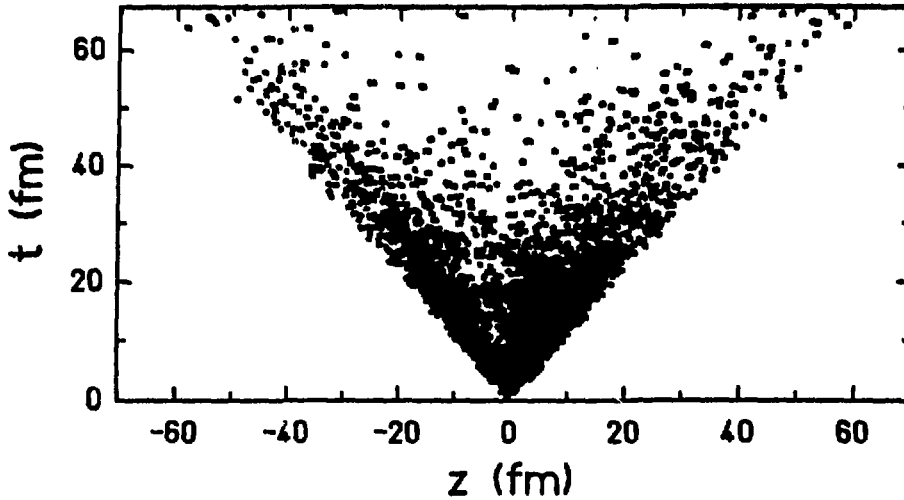


Fig. 22: Spacetime distribution fragment formation in quark jets at $\sqrt{s} = 10$ GeV, measured from the annihilation point in the laboratory frame.

3.5. Applications

Let me discuss briefly just a few numerical results obtained by applying hadron string dynamics to specific processes in hadronic multiparticle production:

3.5.1. *Space-time distribution of particle production:* The mechanism of string decay provides a complete space-time picture of quark jet fragmentation. Fig. 22, where every dot denotes the point of spontaneous creation of a quark-antiquark pair in the flux-tube, shows that the production of the jet fragments is concentrated along the light-cone defined by the endpoints of the string. Plotted in units of the local proper time, most fragments are produced within a few fm/c; hence the “hot” region of space-time is always quite small when viewed from its local rest frame. Experimentally this can be probed by pion-pion correlations in momentum space, which exhibit the characteristic Bose enhancement at relative momenta less than the inverse size of the formation zone. As Fig. 23 shows, the results of string decay simulations agree quite well with the data. [In the simulations the enhancement has been calculated on the basis of the generated space-time distribution of creation points, assuming that these are representative for pions.]

3.5.2. *Multiplicity distributions:* The logarithmic rise of the average jet fragment multiplicity with total available energy is well reproduced by the string decay simulations (see Fig. 26). A more sensitive test of the underlying dynamics is provided by the dependence of the factorial moments of the multiplicity distribution on the

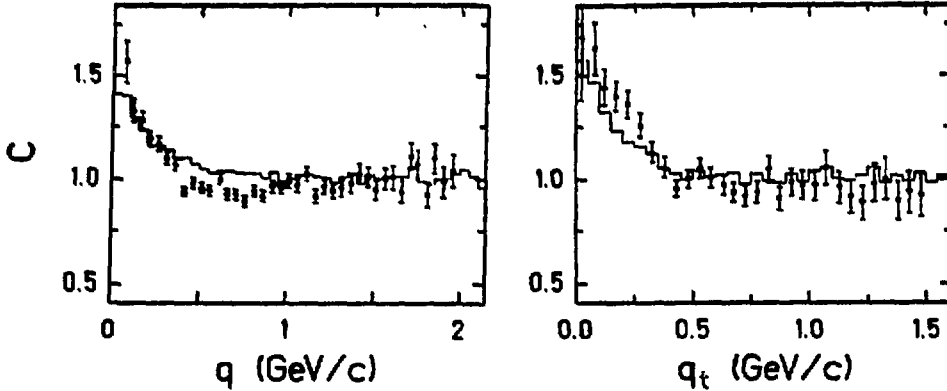


Fig. 23: Correlation function C of like-sign meson pairs as function of invariant momentum difference q (upper part) and of q_T (lower part). [Data: H. Aihara et al. (TPC collab.), Phys. Rev. D31, 996 (1985)].

rapidity bin size. The behavior found in string simulations [38] is very similar to that found in the experimental data, where has been linked to intermittency in the distribution of fragments along the rapidity axis [39]. The origin of this phenomenon may be found in the hierarchical nature of string decay. In fact one finds that the space of fragments exhibits a considerable degree of *ultrametricity* defined as [40]

$$D = 1 - \left(\sum_{i,j} d^<[i,j] \right) / \left(\sum_{i,j} |y_i - y_j| \right), \quad (26)$$

where $d^<[i,j]$ is the largest rapidity gap between fragments i and j .

3.5.3. Relaxation times in hot hadronic matter: Relaxation times for deviations from thermodynamic equilibrium are of great importance in nuclear collisions, since the lifetime of the highly excited fireball is so short. As an example we may ask how fast a gas of nucleons with a thermal energy distribution is expected to approach a hadronic gas with the equilibrium mass distribution. The results of such a simulation [25] are shown in Fig. 24, where the calculated distribution of string masses is shown after four times, corresponding to 1, 2, 10, and 20 times the average collision time between strings, $\tau_0 = [n\langle\sigma\rangle\langle v\rangle]^{-1}$, n being the number density of strings. As you can see, somewhere between $2\tau_0$ and $10\tau_0$ are required to produce an approximately exponential mass distribution which conforms to the laws of equilibrium thermodynamics. The process takes the longer, the further the mass is away from the nucleon mass.

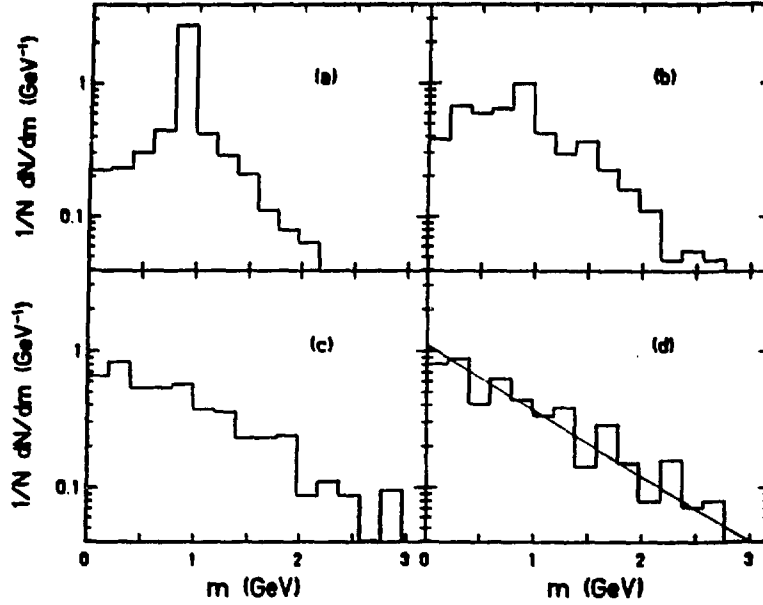


Fig. 24: Rest mass distribution of strings interacting via rearrangement for different values of the time elapsed from the moment of initialization: (a) τ_0 , (b) $2\tau_0$, (c) $10\tau_0$, and (d) $20\tau_0$ (see text). The solid line in figure (d) corresponds to the equilibrium mass distribution.

3.5.4. J/ψ suppression: The lifetime of the charmonium state J/ψ in dense, highly excited hadronic matter is of considerable interest, because a reduction in the number of J/ψ 's produced in a nuclear reaction has been suggested as a signature of quark-gluon plasma creation (see section 2.2). This process been studied in the context of the hadronic string model by Neubauer et al. [41], who calculated the survival rate of a massive charmonium string immersed in an exploding sphere of highly excited massless strings. The motion of a string with massive endpoints in one dimension is given by

$$x(t, \sigma) = (-1)^n \left(\frac{2\sigma}{\pi} - 1 \right) \left\{ \left[(t - 2nt_0)^2 + (m_c/\kappa)^2 \right]^{1/2} - \left[(t_0)^2 + (m_c/\kappa)^2 \right]^{1/2} \right\}, \quad (27)$$

where $m_c = 1.16$ GeV is the charmed quark mass, $M = 3.1$ GeV is the J/ψ mass, and $t_0 = (2\kappa)^{-1} \sqrt{M^2 - 4m_c^2}$ is half the period of oscillation of the $(c\bar{c})$ pair. The J/ψ is quite well described by such a string, with an average $c\bar{c}$ -separation of 0.56 fm. In the collision between the $c\bar{c}$ -string and one of the normal massless strings rearrangement, i.e. formation of a pair of D-mesons, was assumed to occur whenever the total c.m. energy exceeded the DD mass threshold. The hadronic fireball

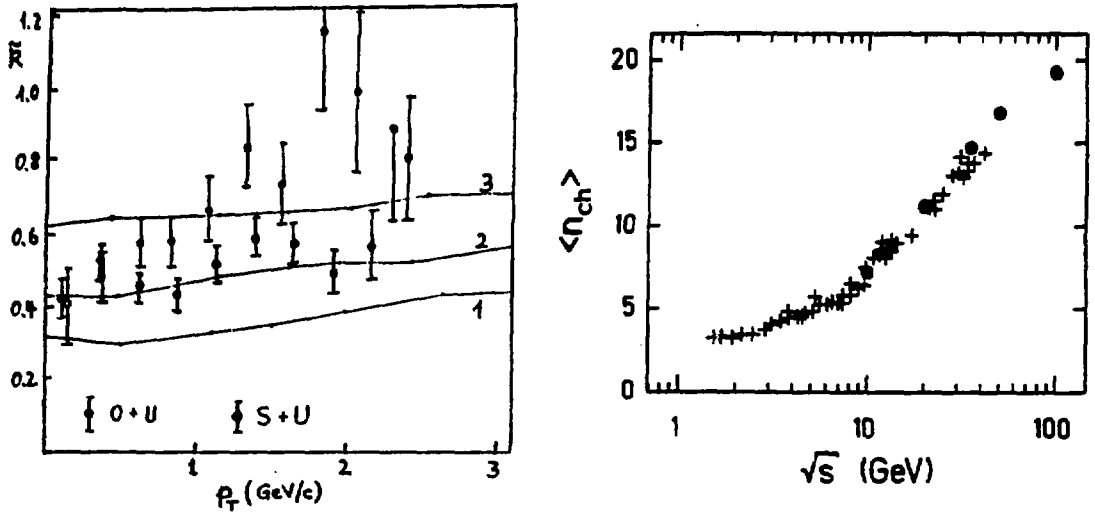


Fig. 25: (left) Suppression of J/ψ formation in an expanding fireball of hadron strings versus transverse momentum of the J/ψ for initial energy densities of 1, 2, and 3 GeV/fm³ (curves 1-3). Also shown are the NA38 data for central O+U and S+U collisions at 200 GeV/u.

Fig. 26: (Right) Total jet multiplicity as function of \sqrt{s} , compared with the data of Mättig et al. (see Fig. 19).

was initialized with various values for the initial energy density and then allowed to expand freely. The simulation was stopped when the density had become so low that further collisions between the $c\bar{c}$ -string and other strings were unlikely. The results in Fig. 25 show that the amount of destruction of $c\bar{c}$ -strings depends strongly on the initial energy density, but only very slightly on the transverse momentum given to the $c\bar{c}$ -string, up to $p_T = 3$ GeV/c. A comparison with experimental data from NA38 shows that an initial energy density of 1.5–2 GeV/fm³ could account for the observed suppression effect. However, the strong dependence on p_T seen in O+U collisions indicates that other effects not described in this simulation, such as parton pre-scattering, may also play a role.

3. HIGGS BOSON PRODUCTION BY FAST NUCLEI

3.1. Two-Photon Physics with Colliding Nuclei

Proton-proton colliders in the multi-TeV energy range will become available toward the end of the coming decade. In principle, these machines will also allow for the acceleration of heavy nuclei, with final energies of 3.5 TeV/u at the

CERN Large Hadron Collider (LHC) and 8 TeV/u at the Superconducting Supercollider (SSC). It has recently been realized [42,43] that such nuclei can be considered as carriers of intense photon "beams" in the energy range relevant for electroweak unification, and hence may serve as tools for probing this region of physics in channels which are not easily accessible in e^+e^- collisions due to their quantum numbers ($J^{PC} \neq 1^{--}$).

As is well known, the electromagnetic field accompanying highly energetic charged particles can be effectively described as an ensemble of high energy photons that are almost on mass shell. In the so-called *equivalent photon approximation* (EPA) the upper bound of readily available photon energies is of the order of the inverse Lorentz contracted radius R of the moving charge:

$$\omega_0 = \gamma/R, \quad (28)$$

where γ is the Lorentz factor of the fast moving particle ($\gamma \approx 3500$ for the LHC and $\gamma \approx 8000$ for the SSC). For Pb nuclei ($R \approx 7$ fm) this implies that virtual photons up to 100 GeV (LHC) or 200 GeV (SSC) would be available. Thus, indeed, c.m. energies of a few hundred GeV can be reached in collisions of two virtual photons contained in the Coulomb fields carried along by the colliding nuclei.

In the framework of the EPA the cross section for production by two virtual photons of a neutral final state f is expressed in the form

$$\sigma_{AA}^f = \int d\omega_1 d\omega_2 n_A(\omega_1) n_A(\omega_2) \int ds \delta(4\omega_1\omega_2 - s) \sigma_{\gamma\gamma}^f(s) \quad (29)$$

where $\sigma_{\gamma\gamma}^f(s)$ is the cross section for producing the final state f in $\gamma\gamma$ -collisions at c.m. energy \sqrt{s} . The function $n_A(\omega)$, which describes the spectral distribution of equivalent photons in the Coulomb field of a moving nucleus of charge Z , is related to the elastic nuclear charge form factor $F_A(k)$ through

$$n_A(\omega) = \frac{2Z^2\alpha}{\pi\omega} \int_{\omega/\gamma}^{\infty} dk \frac{k^2 - (\omega/\gamma)^2}{k^3} F_A(k)^2. \quad (30)$$

The factor Z^2 in Eq.(30) is the main reason why colliding nuclear beams may serve as valuable tool for two-photon physics. The resulting Z^4 -dependence of the cross section makes heavy nuclei more effective than protons or electrons by a factor up to 10^8 . For final states with invariant mass below ω_0 this enhancement far outweighs suppression due to the nuclear form factor. Of course, a large part

of this enhancement must serve to compensate for the much lower luminosity attainable in nuclear colliders (about 10^{28} cm $^{-2}$ versus 10^{33} cm $^{-2}$ in pp-colliders).

In case that the final state is a single neutral particle X^0 with spin $J \neq 1$, the cross section for the process $\gamma\gamma \rightarrow X^0$ is narrowly peaked around the particle mass M_X . It can then be well approximated by:

$$\sigma_{\gamma\gamma}^{X^0}(s) = \frac{8\pi^2}{M_X} \Gamma_{X^0 \rightarrow \gamma\gamma} \delta(s - M_X^2), \quad (31)$$

where $\Gamma_{X^0 \rightarrow \gamma\gamma}$ is the partial two-photon decay width of the produced particle. To discuss the dependence of the production cross section as a function of the neutral particle mass, it is useful to separate phase space factors by writing the decay width in terms of a decay constant $f_X^2 = \alpha^2 M_X^3 / 64\pi^3 \Gamma$. This yields

$$\sigma_{AA}^X = F(M_X) / f_X^2 \quad (32)$$

where $F(M)$ is a universal function depending on $x_0 = M/2\omega_0$:

$$F(M) = \frac{Z^4 \alpha^4}{\pi^3} \int_{x_0}^{\infty} \frac{dx}{x} f(x) f(x_0^2/x). \quad (33)$$

The dimensionless function $F(M)$ is shown in Fig. 27 for several collider energies, the lowest one corresponding to the LHC parameters, the second one being close to the possible SSC specifications. The fact that $\pi^3 F(M)$ is of order one indicates the strength of the two-photon production mechanism in collisions of heavy nuclei, where the coherent action of the total nuclear charge results in an effective electromagnetic coupling strength of order one.

The intensity of photon-photon scattering accompanying the colliding nuclei has an undesired side effect leading to beam loss. Calculations show that roughly 0.03 percent of the total e^+e^- production cross section of about 3×10^5 barn goes into a final state, where the electron is captured by one of the nuclei [44]. In these cases the charge of the beam particle is changed and the ion will be quickly lost in the accelerator. Estimates have indicated that this effect and other beam loss mechanisms will limit the lifetime of a beam of Pb nuclei at several TeV/u and luminosity around 10^{28} cm $^{-2}$ to a few hours [45]. While this is just acceptable, it poses a severe upper limit on the attainable luminosity.

3.2. Higgs Boson Production

Most interesting for fundamental research purposes is the predicted cross section for production of neutral Higgs particles. The reason is that there is a window of possible Higgs masses, $100 \text{ GeV} < m_H < 200 \text{ GeV}$, where detection becomes impossible or very difficult at e^+e^- colliders (for lack of c.m. energy) or pp-colliders (for background reasons) available in the foreseeable future. Peripheral nuclear collisions would provide an ideal environment for new particle searches, because purely electromagnetic scattering results in low-multiplicity final states, especially in the central rapidity region where all created heavy particles would be found.

The two-photon coupling in the standard electroweak model is given by:

$$\Gamma_{H \rightarrow \gamma\gamma} = \frac{\alpha^2}{8\sqrt{2}\pi^3} G_F m_H^3 |I|^2 \quad (34)$$

where G_F is the Fermi constant and m_H is the Higgs mass. The dimensionless parameter I , containing contributions from intermediate lepton, quark, and gauge boson loops, is of order one [46]. In the standard electroweak model with three fermion generations, its value is dominated by contributions from Feynman diagrams involving a virtual W-boson or top quark loop, and is uniquely determined when the Higgs boson and top quark mass are given. Here we adopt a value $m_t = 50 \text{ GeV}$ for the mass of the top quark. As Fig. 28 shows, the cross section for a Higgs mass of 100 GeV rises from 0.15 nb in the LHC energy region up to almost 1 nb at energies available at the SSC. This is almost equal to the cross section predicted for the gluon fusion mechanism $gg \rightarrow H$ in proton-proton collisions at 40 TeV c.m. energy [47]. However, in that case the mechanism requires hadronic scattering and is therefore always accompanied by hadronic multiparticle production. This makes Higgs production much harder to detect at the proton collider, in particular for a low Higgs mass.

The Higgs boson, once it is created will predominantly decay into a $b\bar{b}$ -, a $t\bar{t}$ -, or a W^+W^- pair, depending on its mass. It turns out that the signal-to-background (from direct two-photon production of the pair) ratio is experimentally favorable only when the Higgs is too light to decay into a $t\bar{t}$ - or a W^+W^- pair, because the background of $b\bar{b}$ -pairs is rather small due to the small electric charge ($-\frac{1}{3}e$) of the b-quark [48]. This limits the interesting mass range of the Higgs boson to below 165 GeV .

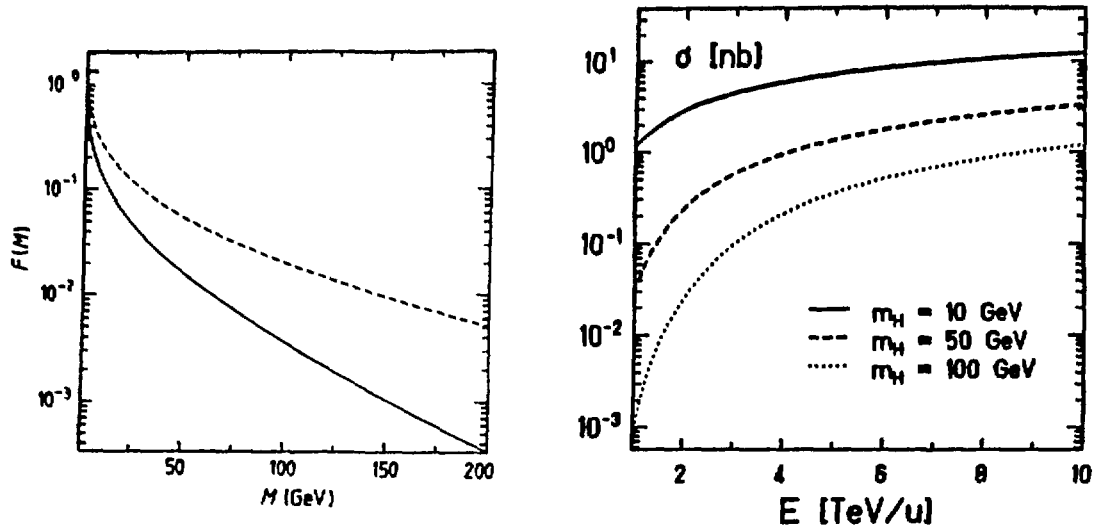


Fig. 27: (Left) The dimensionless function $F(M)$ versus the neutral particle mass M for uranium-uranium collisions at beam energies of 3.5 TeV/n (solid line) and 8 TeV/n (dashed line).

Fig. 28: (Right) Production cross section for Higgs bosons in U+U collisions as function of beam energy and Higgs mass m_H .

Let me note as an aside here that other particles of fundamental interest may also be produced with appreciable cross section, e.g. light technicolor bosons, such as the technipion, or supersymmetric partners of known elementary particles. In pp-collisions at SSC energies (20 TeV on 20 TeV) cross sections for slepton pair production are predicted to be of order 1 pb, while those for photino pair production are even smaller. In the case of charged sleptons in this mass region we expect pair production cross sections in Pb+Pb collisions to be in the range of 1-10 nb [49]. Photino production will be less likely because it involves at least one additional electromagnetic vertex.

There are several questions remaining to be answered before a Higgs search in nuclear collisions can be seriously considered. Besides checks concerning the validity of the equivalent photon approximation, the impact parameter dependence of the cross section must be calculated. It is only in peripheral nuclear collisions, where no hadronic interactions occur, that one stands a chance of detecting the decaying Higgs boson. In the framework of the EPA the impact parameter depen-

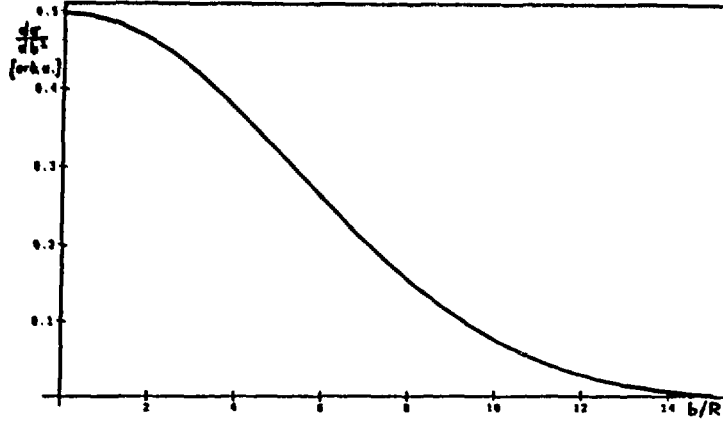


Fig. 29: Impact parameter dependence of Higgs boson production by colliding Pb nuclei at SSC energies (8 TeV/u). The impact parameter b is scaled to the nuclear radius R .

dence is given by a six-dimensional integral over an oscillating integrand:

$$\frac{d\sigma_{AA}^H}{db} = \left(\frac{4Z^2\alpha}{\pi}\right)^2 \frac{\pi b \Gamma_{\gamma\gamma}^H}{m_H} \int d\omega_1 d\omega_2 d^2q e^{i\vec{q}\cdot\vec{b}} \tilde{n}_A(\omega_1, q) \tilde{n}_A(\omega_2, q), \quad (35)$$

with

$$\tilde{n}_A(\omega, q) = \omega^{-1} \int d^2k_T k_T^2 \frac{F(-k^2)F(-(k-q)^2)}{k^2(k-q)^2}, \quad (36)$$

which is difficult to calculate numerically. An approximate semi-analytic evaluation [50] indicates that a sizable part of the production cross section comes from peripheral impact parameters $b > 2R$, but it may be necessary to restrict to $b > 3R$ or so in view of the exponential tail of the nuclear density distribution. As Fig. 29 shows, Pb nuclei at SSC energies are highly preferred due to the much wider b -distribution predicted at the higher energy.

A second open question concerns the contribution of “soft” hadronic interactions leading to $b\bar{b}$ background production without any other distinguishable feature that may be experimentally used to select against such events. Collisions of two virtual pomerons P^0 (double pomeron exchange) is such a mechanism [51]. Even though the process $P^0P^0 \rightarrow b\bar{b}$ has a finite short range, and hence can occur (without other nuclear background) only in grazing nuclear collisions, its much larger strength and its growth with the nuclear surface ($\sigma_{AA} \propto A^{16/9}$) make it a formidable background source. Fortunately, its contribution to direct $b\bar{b}$ -pair production at large transverse momenta ($p_T \approx 50$ GeV/c) will be strongly reduced due

to the internal form factor of the pomeron. Quantitative calculations are urgently needed, but the situation does not look hopeless.

ACKNOWLEDGEMENT

I would like to thank D. Neubauer, K. Sailer, Z. Schram, and A. Schramm for their permission to present various unpublished results.

REFERENCES

1. B. Müller, *The Physics of the Quark-Gluon Plasma*, Lecture Notes in Physics (Springer, Heidelberg 1985).
2. L. McLerran, *Rev. Mod. Phys.* **58**, 1021 (1986).
3. E.V. Shuryak, *The QCD Vacuum, Hadrons, and the Superdense Matter*, (World Scientific, Singapore 1989).
4. J.D. Stack, *Phys. Rev. D* **27**, 412 (1983).
5. R. Fukuda and T. Kugo, *Nucl. Phys. B* **117**, 250 (1976); K. Higashijima, *Phys. Rev. D* **29**, 1228 (1984).
6. see e.g. F. Karsch, *Z. Phys. C* **38**, 147 (1988).
7. S. Gottlieb et al., *Phys. Rev. D* **35**, 3972 (1987).
8. see e.g. C. Alcock et al., *Nucl. Phys. A* **498**, 301c (1989).
9. H.C. Liu and G.L. Shaw, *Phys. Rev. D* **30**, 1137 (1984).
10. C. Greiner, P. Koch, and H. Stöcker, *Phys. Rev. Lett.* **58**, 1825 (1987).
11. see e.g. K. Kajantie and L. McLerran, *Ann. Rev. Nucl. Part. Sci.* **37**, 293 (1987).
12. E.V. Shuryak and O. Zhirov, *Phys. Lett.* **89B**, 253 (1979).
13. L. van Hove, *Phys. Lett.* **118B**, 138 (1982).
14. E.L. Feinberg, *Nuovo Cim.* **34A**, 391 (1976). G. Donnokos and J.I. Goldman, *Phys. Rev. D* **23**, 203 (1981).
15. P.V. Ruuskanen, in: *Quark-Gluon Plasma*, ed. R.C. Hwa (World Scientific, Singapore 1990).
16. T. Matsui and H. Satz, *Phys. Lett.* **178B**, 416 (1986).
17. J.Y. Grossiord et al. [NA38 collab.], *Nucl. Phys. A* **498**, 249c (1989).
18. J.P. Blaizot, *Nucl. Phys. A* **498**, 272~ (1989).

19. S. Gavin and R. Vogt, preprint LBL-27417, Berkeley (1990).
20. J. Rafelski and B. Müller, *Phys. Rev. Lett.* **48**, 1066 (1982).
21. P. Koch, B. Müller, and J. Rafelski, *Phys. Rep.* **142**, 167 (1986).
22. T. Abbott et al. [E802 collab.], *Nucl. Phys.* **A498**, 67c (1989).
23. M. Gazdzicki et al. [NA35 collab.], *Nucl. Phys.* **A498**, 375c (1989).
24. R. Mattiello, H. Sorge, H. Stöcker, and W. Greiner, *Phys. Rev. Lett.* **63**, 1459 (1989).
25. K. Sailer, W. Greiner, and B. Müller, in: *Quark-Gluon Plasma*, ed. R.C. Hwa (World Scientific, Singapore 1990).
26. R. Hagedorn, *Suppl. Nuovo Cim.* **3**, 147 (1965).
27. R. Hagedorn and J. Rafelski, *Phys. Lett.* **97B**, 136 (1980).
28. G. Veneziano, *Phys. Rep.* **9**, 199 (1974).
29. see e.g. J. Scherk, *Rev. Mod. Phys.* **47**, 123 (1975).
30. K. Sailer, B. Müller, and W. Greiner, *Int. J. Mod. Phys.* **A4**, 437 (1989).
31. see e.g. M.B. Green, J.H. Schwarz, and E. Witten, *Superstring Theory*, Chapt. 7 (Cambridge Univ. Press, 1987).
32. T. Schönfeld et al., *Pair creation in a flux tube*, preprint, Frankfurt (1989).
33. K. Sailer, T. Schönfeld, A. Schäfer, B. Müller, and W. Greiner, UFTP preprint 244, Frankfurt (1990).
34. E. Remler, *Proceed. Int. Workshop, Hirschegg* (1989).
35. M. Strayer et al., Oak Ridge, private communication.
36. K. Sailer, B. Müller, and W. Greiner, *Space-time picture of quark fragmentation*, preprint, Frankfurt (1989).
37. Z. Schram, K. Sailer, B. Müller, and W. Greiner, *Boson interferometry in string fragmentation*, preprint, Frankfurt (1989).
38. K. Sailer et al., Frankfurt, to be published.
39. A. Bialas and R. Peschanski, *Nucl. Phys.* **B308**, 803 (1988).
40. R. Rammal, G. Toulouse, and M.A. Virasoro, *Rev. Mod. Phys.* **58**, 765 (1986).
41. D. Neubauer et al., *Mod. Phys. Lett.* **A4**, 1627 (1989), and to be published.
42. M. Grabiak, B. Müller, W. Greiner, G. Soff, and P. Koch, *J. Phys.* **G15**, L25 (1989) [GSI preprint 87-78].

43. E. Papageorgiu, *Phys. Rev.* **D40**, 92 (1989); *Nucl. Phys.* **A498**, 493c (1989).
44. G. Baur and C.A. Bertulani, *Nucl. Phys. A*, in print.
45. D. Brandt, *Relativistic heavy ions in the LHC*, LHC Note No. 87, CERN (1989).
46. J. Ellis, M.K. Gaillard, and D.V. Nanopoulos, *Nucl. Phys.* **B106**, 292 (1976); R. Bates and J.N. Ng, *Phys. Rev.* **D33**, 657 (1985).
47. E. Eichten et al., *Rev. Mod. Phys.* **56**, 579 (1984).
48. M. Drees, J. Ellis, and D. Zeppenfeld, *Phys. Lett.* **B223**, 454 (1989).
49. J. Rau, B. Müller, W. Greiner, and G. Soff, *J. Phys.* **G**, in print.
50. A. Schramm, Duke University, private communication.
51. see e.g. D.M. Chew and R. Shankar, *Phys. Rev.* **D11**, 1036 (1975).